

Quantum Scrambling Born Machine

Marcin Płodzień^{1,*}

¹*Qilimanjaro Quantum Tech, Carrer de Venezuela 74, 08019 Barcelona, Spain*

(Dated: February 20, 2026)

Quantum generative modeling, where the Born rule naturally defines probability distributions through measurement of parameterized quantum states, is a promising near-term application of quantum computing. We propose a Quantum Scrambling Born Machine in which a fixed entangling unitary—acting as a scrambling reservoir—provides multi-qubit entanglement, while only single-qubit rotations are optimized. We consider three entangling unitaries—a Haar random unitary and two physically realizable approximations, a finite-depth brickwork random circuit and analog time evolution under nearest-neighbor spin-chain Hamiltonians—and show that, for the benchmark distributions and system sizes considered, once the entangler produces near-Haar-typical entanglement the model learns the target distribution with weak sensitivity to the scrambler’s microscopic origin. Finally, promoting the Hamiltonian couplings to trainable parameters casts the generative task as a variational Hamiltonian problem, with performance competitive with representative classical generative models at matched parameter count.

I. INTRODUCTION

Quantum machine learning (QML) exploits quantum resources—superposition, entanglement, and the exponential dimensionality of Hilbert space—to enhance learning tasks [1–9], with quantum generative models emerging as a promising near-term application [10–14]. Quantum generative models take inspiration from their classical counterparts, such as quantum generative adversarial networks (qGANs) [15–18] and quantum diffusion models [19, 20].

A conceptually distinct family are quantum circuit Born machines (QCBMs), in which a parametrized quantum state is measured in the computational basis, with the Born rule naturally defining a normalized probability distribution over exponentially many outcomes [21–23]. Born machines can provably achieve an exponential representational advantage over classical generative models [24], and subsequent work has benchmarked QCBMs on financial and synthetic datasets, including their generalization properties [25–28].

Quantum Born machines, like other variational quantum algorithms, face a tradeoff between expressivity and trainability of the parametric ansatz [6]. Highly expressive circuits, such as deep random parametric architectures, can in principle represent any target distribution; however, they suffer from barren plateaus, where gradients of the loss function vanish exponentially with system size, rendering optimization infeasible [29–31]. Shallow or overly structured circuits may lack the entangling power to represent complex target distributions faithfully [32, 33].

In this work we propose a Quantum Scrambling Born Machine (QSBM), in which we decouple entanglement generation from the trainable degrees of freedom. We treat quantum scrambling—the rapid spread of initially

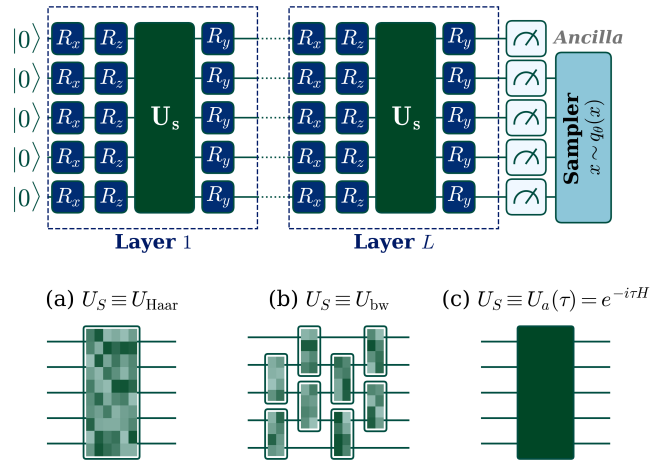


FIG. 1. Architecture of the quantum scrambling Born machine. An N -qubit register, initialized in $|0\rangle^{\otimes N}$, is processed through L repeated layers; each layer applies trainable single-qubit rotations (\hat{R}_x, \hat{R}_z before, \hat{R}_y after) surrounding a fixed scrambling unitary \hat{U}_S that generates entanglement. After L layers, N_A ancilla qubits are traced out and the remaining $n = N - N_A$ system qubits are measured in the computational basis, producing a probability distribution via the Born rule [Eq. (2)]. Only the rotation angles are optimized; the scrambler is kept fixed. Three scrambler types are considered: (a) Haar random unitary, (b) brickwork random quantum circuit (RQC) of depth K , (c) analog Hamiltonian evolution $e^{-i\tau \hat{H}}$.

localized quantum information across all degrees of freedom of a many-body system [34–39]—as an entangling resource for quantum generative modeling: once the fixed unitary produces Haar-typical bipartite entanglement, diagnosed by the half-chain von Neumann entropy approaching the Page value [40], representation learning is controlled entirely through single-qubit rotations, see Fig. 1. The entangling layer is provided by either an ideal

* marcin.plodzien@qilimanjaro.tech

Haar random unitary or its physical approximations—finite-depth brickwork random circuits on digital platforms and finite-time Hamiltonian evolution on analog quantum simulators. Because the scrambler is a fixed, non-trainable unitary reused in every layer, it needs to be calibrated or compiled only once; the entire trainable parameter budget is devoted to single-qubit rotations, making the architecture particularly suited to near-term hardware where multi-qubit gate recalibration is the dominant overhead.

We monitor the generative performance from under-scrambled to fully scrambled regimes and find that, for the qubit counts ($N \leq 10$) and target families studied here, the converged model quality is controlled by how closely the entangler’s bipartite entanglement approaches the Haar-typical value. For a fixed qubit budget, tracing out ancilla qubits increases expressivity by exploring mixed-state distributions. Extending the architecture to trainable Hamiltonian couplings casts the generative task as a variational Hamiltonian problem, complementing the inverse Hamiltonian learning problem [41–51]. A comparison with representative classical generative models—a GAN, a variational autoencoder (VAE), and a restricted Boltzmann machine (RBM)—at matched parameter count indicates that the QSBM is competitive in the small trainable-parameter regime.

The remainder of the paper is organized as follows. Section II introduces the model architecture, the role of scrambling and Haar typicality. Section III describes the training protocol, loss function, and target distributions. Section IV presents the main results for Haar, digital, and analog scramblers. Section V extends the architecture to trainable Hamiltonian parameters and benchmarks it against classical generative models. We conclude in Sec. VI.

II. MODEL

A. Quantum Born machines

A quantum Born machine is a generative model that encodes a probability distribution in the squared amplitudes of a quantum state [21, 22]. Given N qubits, we prepare a parameterized state by applying L identical structural layers to the reference state $|0\rangle^{\otimes N}$. Each layer $\ell = 1, \dots, L$ consists of trainable single-qubit pre-rotations $\hat{R}_x(\theta_{i,x}^{(\ell)}) \hat{R}_z(\theta_{i,z}^{(\ell)})$ applied to every qubit i , followed by a fixed scrambling unitary \hat{U}_S , and concluded by a trainable post-rotation $\hat{R}_y(\theta_{i,y}^{(\ell)})$ on every qubit. The full circuit unitary reads

$$\hat{U}(\boldsymbol{\theta}) = \prod_{\ell=1}^L \hat{R}_{y,\text{post}}^{(\ell)} \hat{U}_S \hat{R}_{z,\text{pre}}^{(\ell)} \hat{R}_{x,\text{pre}}^{(\ell)}, \quad (1)$$

where the product is ordered with $\ell = 1$ applied first (rightmost), the rotation operators act independently on

each qubit, $\hat{R}_{\alpha,\text{pre/post}}^{(\ell)} = \bigotimes_{i=1}^N \hat{R}_\alpha(\theta_{i,\alpha}^{(\ell)})$, and each angle $\theta_{i,\alpha}^{(\ell)}$ is an independently trained parameter. The same scrambling unitary \hat{U}_S is reused in every layer, modeling a fixed entangling reservoir—analogous to the reservoir-computing paradigm, where a complex dynamical system is probed through simple, trainable readout layers. Reuse also reflects the hardware-relevant scenario in which the entangling operation is calibrated or compiled once and held fixed, so that only single-qubit control pulses are adjusted during training. What distinguishes successive layers are their independently trained rotation angles. The resulting state $|\psi(\boldsymbol{\theta})\rangle = \hat{U}(\boldsymbol{\theta})|0\rangle^{\otimes N}$ is measured in the computational basis. For $N_A = 0$ (no ancillas), every qubit is measured and outcome $x \in \{0, 1\}^N$ occurs with probability

$$q_{\boldsymbol{\theta}}(x) = |\langle x | \psi(\boldsymbol{\theta}) \rangle|^2. \quad (2)$$

The total number of trainable parameters is $3LN$ (three rotation angles per qubit per layer), scaling linearly in both L and N . When N_A ancilla qubits are included, they participate in the scrambling but are traced out before measurement. Defining the reduced density matrix $\hat{\rho}_{\text{sys}} = \text{Tr}_A[|\psi(\boldsymbol{\theta})\rangle\langle\psi(\boldsymbol{\theta})|]$, the output probability is

$$q_{\boldsymbol{\theta}}(x) = \langle x | \hat{\rho}_{\text{sys}} | x \rangle = \sum_{a \in \{0, 1\}^{N_A}} |\langle x, a | \psi(\boldsymbol{\theta}) \rangle|^2, \quad (3)$$

where $x \in \{0, 1\}^n$ labels computational-basis states of the measured register of size $n = N - N_A$. Since $\hat{\rho}_{\text{sys}}$ has rank at most 2^{N_A} , its spectral decomposition expresses the output distribution as a convex combination of up to 2^{N_A} pure-state Born distributions, enlarging the representable class beyond a single pure state.

B. Quantum scrambling and Haar typicality

Entanglement and many-body correlations are essential for the expressivity of quantum generative models, since a product-state circuit can only produce factorized output distributions. The ideal scrambling unitary is a Haar-random unitary \hat{U}_{Haar} , drawn from the unique unitarily invariant measure on $U(2^N)$ [39, 52], which maps an initial product state $|0\rangle^{\otimes N}$ to a state whose quantum information is delocalized across all degrees of freedom [34]. A key property of such states is typicality [53, 54], i.e. almost every Haar-random state is nearly maximally entangled across any bipartition, with the average bipartite entropy given by the Page formula [40], $\langle S_A \rangle_{\text{Haar}} = \sum_{k=d_B+1}^{d_A d_B} k^{-1} - (d_A - 1)/(2d_B) \approx \ln d_A$ (where $d_A d_B = 2^N$, $d_B \geq d_A$), and fluctuations around this value exponentially suppressed in N . When N_A ancilla qubits are traced out from a Haar-scrambled state, the reduced density matrix $\hat{\rho}_{\text{sys}}$ follows the fixed-trace Wishart distribution [55] with generically non-degenerate eigenvalues.

Implementing a true Haar-random unitary requires a gate count that grows with N [56], making it impractical beyond small system sizes. Two physically realizable strategies approximate Haar-level scrambling. (i) Random quantum circuits of depth K in a brickwork layout converge to approximate unitary t -designs—ensembles whose first t moments match those of the Haar measure. Already at $t = 2$, coarse entanglement properties such as subsystem purities and Rényi-2 entropies become indistinguishable from the Haar ensemble [57–62]. (ii) Analog time evolution under a many-body Hamiltonian produces effective scrambling at sufficiently long times, with the entanglement entropy approaching the Page value [39, 63, 64].

Both approximations are expected to produce Haar-typical entanglement at sufficient depth or evolution time, with subsystem entropies converging to the Page value. In practice, we benchmark each scrambler against the generative performance of a Haar-random unitary $\hat{U}_S = \hat{U}_{\text{Haar}}$.

III. TRAINING AND EVALUATION PROTOCOL

We train the Born machine by minimizing the negative log-likelihood (NLL),

$$\mathcal{L}_{\text{NLL}}(\boldsymbol{\theta}) = - \sum_x p(x) \ln q_{\boldsymbol{\theta}}(x), \quad (4)$$

where $p(x)$ is the target distribution. The NLL is related to the Kullback–Leibler divergence (KLD) by $D_{\text{KL}}(p||q_{\boldsymbol{\theta}}) = \mathcal{L}_{\text{NLL}}(\boldsymbol{\theta}) - H(p)$, where $H(p)$ is the Shannon entropy of the target [65]. Since $H(p)$ is constant, minimizing NLL is equivalent to minimizing D_{KL} , our primary performance metric.

For the one-dimensional benchmarks (Secs. IV A–IV C), we employ a multimodal distribution composed of five Gaussian peaks discretized onto 2^n bins (where $n = N - N_A$ is the number of measured system qubits):

$$p(x) \propto \sum_{j=1}^5 w_j \exp \left[-\frac{(x - \mu_j)^2}{2\sigma^2} \right], \quad (5)$$

where the peak centers are uniformly spaced at $\mu_j = (j - 0.5) \cdot 2^n/5$ for $j = 1, \dots, 5$, the common width is $\sigma = 2^n/20$, and the weights w_j are drawn randomly from $U(0.5, 1.5)$ with a fixed seed to ensure reproducibility. The unequal heights and sharp inter-peak valleys make this a non-trivial benchmark for the model.

For the two-dimensional benchmarks (Sec. V), the N qubits are split into two registers of $n_x = n_y$ system qubits, each mapped to the interval $[-3, 3]$ and discretized onto a $2^{n_x} \times 2^{n_y}$ grid. We study two target distributions. (i) A bivariate Gaussian with tunable correlation,

$$p(x, y) \propto \exp \left[-\frac{x^2 - 2\rho xy + y^2}{2(1 - \rho^2)} \right], \quad (6)$$

with $\rho \in \{0, 0.5, 0.9\}$. (ii) A mixture of four isotropic Gaussians,

$$p(x, y) \propto \sum_{k=1}^4 \exp \left[-\frac{(x - \mu_{x,k})^2 + (y - \mu_{y,k})^2}{2\sigma^2} \right], \quad (7)$$

with centers $(\mu_{x,k}, \mu_{y,k}) \in \{(\pm 1.5, \pm 1.5)\}$ and $\sigma = 0.5$.

IV. QUANTUM SCRAMBLING AS A GENERATIVE RESOURCE

Unless otherwise noted, all one-dimensional experiments use $N = 8$ total qubits, are trained for 2000 epochs and averaged over 20 independent realizations (each with a freshly drawn scrambler instance and random initial parameters); error bars denote $\pm 1\sigma$. Optimization uses Adam [66] (learning rate 0.01, gradient norm clipping at 1.0) with exact autodiff gradients computed from the full statevector probabilities. The reported KLD is evaluated from empirical distributions obtained via $N_{\text{shots}} = 5000$ Born-rule samples.

A. Haar random unitary

We begin with the idealized case $\hat{U}_S = \hat{U}_{\text{Haar}}$. Since the scrambler already provides near-maximal entanglement, any remaining limitation in the learned distribution originates from the expressivity of the rotation layers.

Figure 2(a) shows the converged KLD as a function of the number of layers L , with separate curves for $N_A = 0, 1, 2$ ancilla qubits. The KLD decreases monotonically with L , as the number of trainable rotation gates controls the expressivity at fixed scrambler entanglement. For the pure-state case, $N_A = 0$, the model already learns the target distribution well for $L \geq 6$. However, for shallow circuits, $L \leq 5$, tracing out ancilla qubits $N_A = 1, 2$ improves the model expressivity. Panels (b)–(e) illustrate this progression for $N_A = 2$: at $L = 2$ only the coarse envelope of the target is captured, while by $L = 8$ the learned and target distributions agree quantitatively.

Tracing out ancilla qubits simultaneously increases the mixed-state rank of $\hat{\rho}_{\text{sys}}$ and reduces the output register from 2^n to 2^{n-1} bins, so the KLD improvement combines a genuine expressivity gain with a lower-dimensional learning task. At fixed N , increasing N_A trades output resolution for mixed-state expressivity; we focus on this hardware-relevant tradeoff. A controlled comparison at fixed n would isolate rank effects and is a natural extension.

B. Random quantum circuit of depth K

Next, we replace the global Haar unitary with a random quantum circuit of variable depth K arranged in a brickwork topology. Each brickwork layer applies

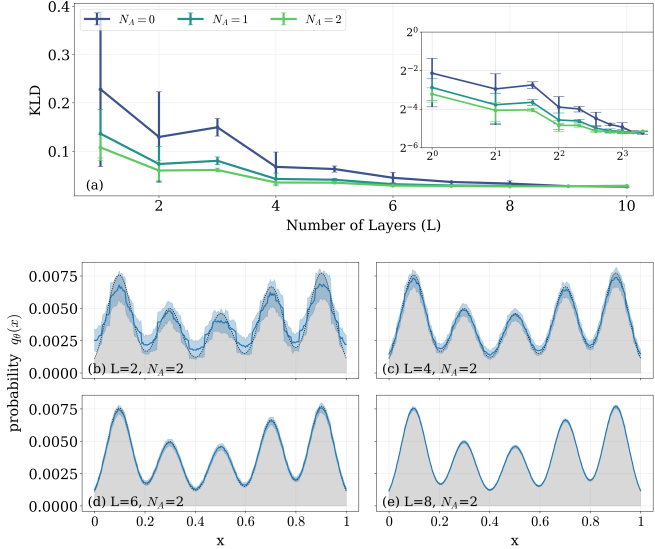


FIG. 2. Born machine performance with a Haar-random scrambler ($N = 8$, $N_{\text{shots}} = 5000$). (a) Converged KLD vs. number of layers L for $N_A = 0, 1, 2$ ancilla qubits. The KLD decreases monotonically with L (inset, log scale), with each additional ancilla qubit shifting the curve downward by roughly one order of magnitude. (b)–(e) Target distribution (gray) vs. learned Born-machine output (blue) at $N_A = 2$ for $L = 2, 4, 6, 8$, illustrating progressive convergence from a coarse to a near-exact reproduction of the multimodal target. Shaded bands: $\pm 1\sigma$ over 20 independent realizations (each with a fresh Haar draw and random initial rotation parameters).

random two-qubit Haar gates to alternating nearest-neighbor pairs. Since a circuit of depth $K \propto N$ is expected to converge to an approximate 2-design [57, 58], the question is how rapidly the Born machine performance tracks this convergence.

Fig. 3 presents the converged KLD as a function of layers L , for given brickwork circuit depth K , with $N_A = 0, 1, 2$ traced-out ancilla qubits (panels (a–c)). At $K = 1$ only nearest-neighbor entanglement is generated, insufficient to scramble the full register, and the KLD saturates regardless of L . Already at $K = 2$ the improvement is substantial, and for $K \geq 5$ all curves collapse onto the Haar-scrambler level. Consistently, the mixed-state expressivity after tracing N_A ancilla qubits improves the model.

C. Analog Hamiltonian scrambler

In this section we consider the entangling layer as a continuous Hamiltonian evolution, $\hat{U}_S = \hat{U}_a(\tau) = e^{-i\tau\hat{H}}$, providing an experimentally relevant scrambling resource on analog quantum simulators, where native many-body dynamics serve as the entangling reservoir, bypassing compiled gate sequences.

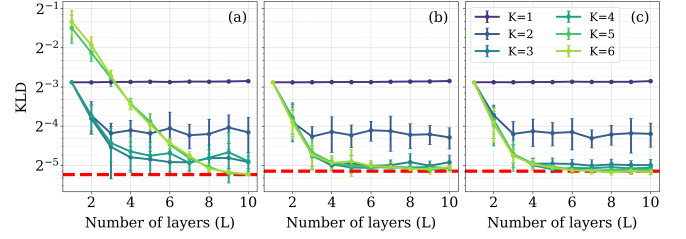


FIG. 3. Finite-depth brickwork random circuit scrambler ($N = 8$, $N_{\text{shots}} = 5000$). Converged KLD vs. number of layers L for brickwork depths $K = 1–6$ at (a) $N_A = 0$, (b) $N_A = 1$, (c) $N_A = 2$. At $K = 1$ the circuit generates only nearest-neighbor entanglement and the KLD saturates well above the Haar-scrambler level (red dashed); by $K \geq 3 \approx N/2$ every curve collapses onto the Haar level, consistent with the theoretical expectation that brickwork circuits of depth $O(N)$ converge to approximate 2-designs and reproduce the entanglement properties of a full Haar-random unitary [58]. Ancilla qubits shift the entire KLD surface downward by roughly one order of magnitude per ancilla. Mean $\pm 1\sigma$ over 20 random circuit instances.

We consider the general nearest-neighbor Hamiltonian

$$\hat{H} = - \sum_{\langle i,j \rangle} (J_{xx} \hat{\sigma}_i^x \hat{\sigma}_j^x + J_{yy} \hat{\sigma}_i^y \hat{\sigma}_j^y + J_{zz} \hat{\sigma}_i^z \hat{\sigma}_j^z) - \sum_i h_x \hat{\sigma}_i^x, \quad (8)$$

where $\hat{\sigma}_i^x, \hat{\sigma}_i^y, \hat{\sigma}_i^z$ are the Pauli operators acting on site i , the sums $\langle i,j \rangle$ run over nearest neighbors under open boundary conditions, and the parameters $J_{\alpha\alpha}$ and h_x define the interaction and field strengths.

We consider two models: the transverse-field Ising model (TFIM), with $J_{zz} = h_x = 1$,

$$\hat{H}_{\text{TFIM}} = - \sum_i \hat{\sigma}_i^z \hat{\sigma}_{i+1}^z - \sum_i \hat{\sigma}_i^x, \quad (9)$$

and the XX model with transverse field, $J_{xx} = J_{yy} = h_x = 1$,

$$\hat{H}_{\text{XX}} = - \sum_i (\hat{\sigma}_i^x \hat{\sigma}_{i+1}^x + \hat{\sigma}_i^y \hat{\sigma}_{i+1}^y) - h_x \sum_i \hat{\sigma}_i^x. \quad (10)$$

Both are integrable models, which map to free fermions via the Jordan–Wigner transformation [67]. However, the trainable local rotations $\hat{R}_\alpha(\theta_{\alpha,i}^{(l)})$, $\alpha = x, y, z$, at each layer l can be viewed as local fields, $h_{\alpha,i}^{(l)} = \theta_{\alpha,i}^{(l)}/\tau$, which break the models’ integrability.

In the following, we study QSBM performance as a function of evolution time τ , for given number of layers L , and ancilla qubits N_A . Figure 4 shows the converged KLD as a function of evolution time τ for $L = 1–8$ layers and $N_A = 0, 1, 2$ ancillas, with the TFIM in the top row and the XX model in the bottom row.

At short evolution times ($\tau \ll 1$), $\hat{U}_a(\tau) \approx \hat{\mathbb{I}} - i\tau\hat{H}$ generates minimal entanglement, and the KLD saturates regardless of L or Hamiltonian type. As τ increases, both models undergo a transition in which the KLD drops

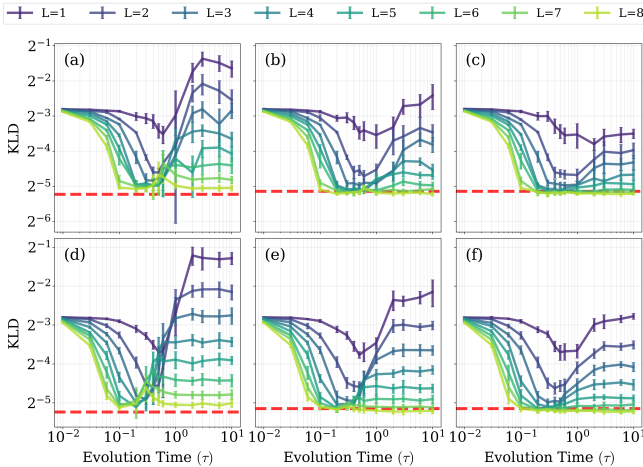


FIG. 4. Analog Hamiltonian scramblers ($N = 8$, $N_{\text{shots}} = 5000$). Converged KLD vs. evolution time τ for $L = 1\text{--}8$ layers (colored lines). Columns: Ancilla qubits $N_A = 0, 1, 2$. Top row (a–c): Transverse-field Ising model [Eq. (9)]—the KLD drops at intermediate $\tau \geq 0.1$ for $L > 5$. Bottom row (d–f): XX model with transverse field [Eq. (10)]—the KLD drops at $\tau \geq 0.1$. Both Hamiltonians for $L \geq 5$ saturate at the Haar-scrambler KLD (red dashed) for $N_A = 1, 2$ ancilla qubits. The role of ancilla qubits is most visible for shallow circuits ($L < 3$) for both Hamiltonians.

sharply around $\tau \sim 0.5$ (in units of the inverse coupling strength), coinciding with the half-chain entropy approaching the Page value.

The shallow circuits ($L \leq 4$) exhibit a non-monotonic dip-type dependence of the KLD on τ , where layers of local rotations do not provide sufficient variational freedom to map such a featureless state onto a structured target, and the KLD increases. For deeper circuits, $L \geq 5$, the additional layers compensate for the excess entanglement and the non-monotonicity disappears. The quantum state is driven toward the maximally scrambled scenario, achieving performance consistent with the Haar limit (horizontal red dashed lines).

Consistently, allocating more qubits to the ancilla register (columns correspond to $N_A = 0, 1, 2$ from left to the right) enlarges the traced-out environment, so the scrambler-generated entanglement translates into a higher-rank mixed state of the sampler and a lower KLD across all τ and L .

We note that the architecture confines trainable parameters to single-qubit rotations, while the entangling unitary is fixed and does not contribute gradients. Empirically, training converges reliably across all 20 random initializations for every configuration tested (up to $N = 10$). However, because the NLL effectively acts as a global cost function [30] and the fixed scrambler can approximate a Haar-random unitary, standard results [31] imply that barren plateaus will set in at sufficiently large N . The reliable convergence observed here is attributed to the intermediate system sizes, where the gradient variance remains within the resolution of the optimizer. A

systematic scaling study of gradient magnitudes with N is an important direction for future work.

V. HAMILTONIAN-DRIVEN GENERATIVE MODELING

We now extend the architecture by promoting the Hamiltonian parameters to trainable variables, replacing the pre- and post-rotation layers with trainable on-site fields $h_{x,i}^{(\ell)}$, $h_{y,i}^{(\ell)}$, $h_{z,i}^{(\ell)}$ —which are equivalent to arbitrary single-qubit rotations at fixed evolution time—and adding a single trainable nearest-neighbor coupling $J_{xx}^{(\ell)}$ per layer. Since the local fields can absorb any global rescaling, a trainable $J_{xx}^{(\ell)}$ at fixed τ effectively controls the entangling strength per layer; with free local fields the rescaling is partly redundant, but in the discrete-layer ansatz the coupling and field parameters are not fully equivalent.

In contrast to the previous scramblers, where a single fixed unitary is reused in every layer, here each layer generates entanglement with an independently optimized coupling strength. The full evolution thus corresponds to L unitary evolutions driven by piecewise-constant Hamiltonians (computed via exact matrix exponentiation), where the initial product state is transformed into a final state whose Born-rule sampling in the computational basis reproduces the target distribution.

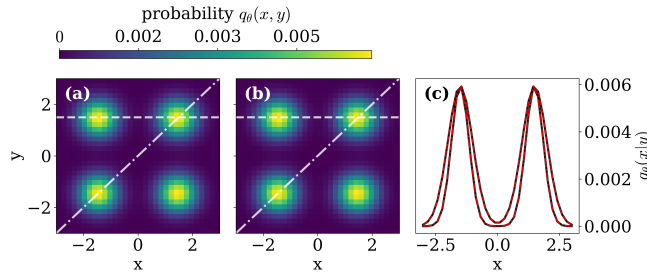
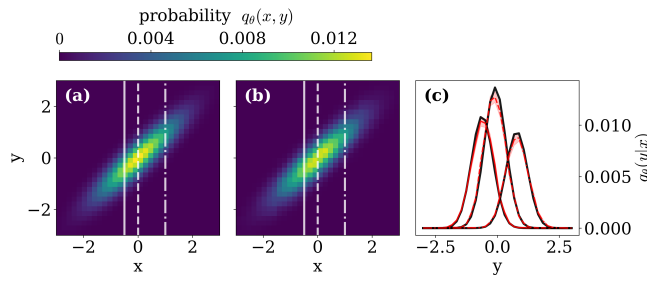
We test this variant on joint probability distributions $p(x, y)$ over two continuous variables. The $N = 10$ qubits (including $N_A = 2$ ancillas) are partitioned into two registers of $n_x = n_y = 4$ system qubits each; tracing out the ancillas yields a $2^{n_x} \times 2^{n_y}$ probability distribution.

We first consider the correlated bivariate Gaussian of Eq. (6) with $\rho = 0.9$, which tests the model’s ability to reproduce non-trivial inter-register correlations. Figure 5 shows that the trainable-Hamiltonian QSBM faithfully captures both the elongated shape and the off-diagonal tilt of the target: panels (a) and (b) are visually indistinguishable, and the conditional slices in panel (c) confirm quantitative agreement at three representative cuts through the distribution.

The multimodal target of Eq. (7) poses a more stringent test, as disconnected modes are notoriously prone to mode collapse in adversarial training [16]. The QSBM captures all four modes with correct relative weights (Fig. 6), as confirmed by the conditional slices in panel (c).

Benchmark against classical models

To assess the competitiveness of the QSBM, we compare the trainable-Hamiltonian variant with three representative classical architectures [68]—a generative adversarial network (GAN) [69], a variational autoencoder (VAE) [70], and a restricted Boltzmann machine



(RBM) [71]—each constrained to approximately 310 trainable parameters, the budget of the considered QSBM architecture, and trained for 50 000 epochs with the Adam optimizer[72].

At this matched parameter budget, the training dynamics reveal differences among the QSBM and the considered classical models (Fig. 7). The top panel presents the mean KLD, averaged over 20 variational parameter initializations, vs. training epoch for each model. The GAN exhibits large seed-to-seed variance and frequent mode collapse, reflecting the fragility of adversarial training at this parameter scale [69]. The VAE converges reliably but produces axis-aligned, broadened peaks—artifacts of the Gaussian decoder and the KL regularization term that penalizes sharp latent encodings. The RBM achieves the lowest KLD among the classical mod-

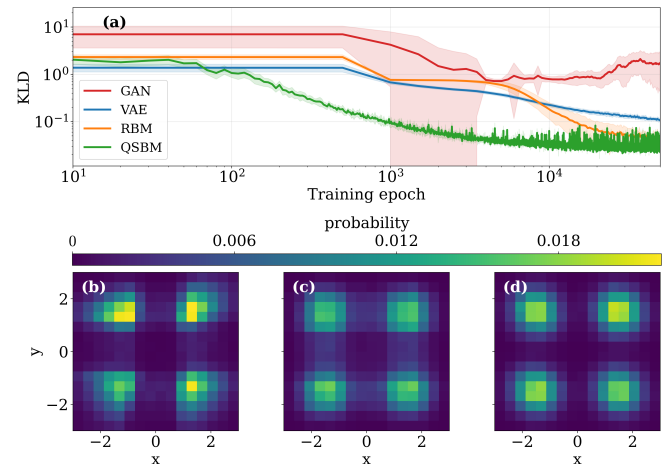


FIG. 7. Top panel (a): KLD vs. training epoch for the trainable-Hamiltonian QSBM (310 params), a generative adversarial network (GAN), a variational autoencoder (VAE), and a restricted Boltzmann machine (RBM) on the multimodal target of Fig. 6, with matched parameter budgets (≈ 310) and 50 000 training epochs (mean $\pm 1\sigma$ over 20 realizations; log-log scale). Bottom panels: representative learned densities from the best-performing seed of each classical model. (b) GAN (302 params; mean KLD: 1.74 ± 1.30). (c) VAE (306 params; mean KLD: 0.11 ± 0.01). (d) RBM (308 params; mean KLD: 0.045 ± 0.008). The QSBM (310 params) achieves a mean KLD of 0.030 ± 0.005 .

els.

The QSBM distribution is normalized by construction via the Born rule, whereas classical models must enforce normalization explicitly (RBM partition function) or learn it implicitly (GAN, VAE evidence lower bound). At matched budget, entanglement and exact Born-rule normalization give the QSBM a competitive advantage over these representative small-capacity baselines; this advantage is expected to narrow as the parameter count grows and classical models gain sufficient capacity.

VI. SUMMARY AND CONCLUSIONS

We have introduced a Quantum Scrambling Born Machine architecture that treats quantum scrambling—operationally defined here as the generation of Haar-typical bipartite entanglement—as a computational resource, where a fixed, non-trainable unitary generates all the entanglement while only single-qubit rotations are optimized. We considered an ideal Haar-random unitary and its two experimentally feasible approximations: finite-depth brickwork random circuits and analog evolution under nearest-neighbor spin-chain Hamiltonians. For the benchmark distributions and system sizes studied ($N \leq 10$), once the entangling unitary approaches Haar-typical entanglement, the learned distribution closely matches the target with weak sensitivity to the scrambler’s microscopic origin. In the fixed-

scrambler variant, the scrambler provides entanglement at zero trainable cost, so the entire parameter budget is devoted to expressivity, making the architecture particularly parameter-efficient and well suited to near-term platforms where the entangling operation—whether a native gate sequence or analog many-body dynamics—can be calibrated once and reused. Tracing out ancilla qubits allows the model to explore mixed-state distributions, increasing its expressivity at fixed qubit budget. This observation suggests that noise inevitably present on physical hardware can be treated as an additional expressivity resource [73], naturally introducing mixedness.

Finally, the trainable-Hamiltonian variant shows that Hamiltonian parameters can be optimized so that a piecewise-constant evolution, starting from a product state, generates a quantum state whose Born-rule mea-

surement statistics reproduce a target classical probability distribution. This casts many-body quantum dynamics as a programmable generative resource, complementing the inverse Hamiltonian learning problem—where unknown couplings are inferred from measurements—with a forward generative counterpart in which Hamiltonian parameters are optimized to reproduce a target classical distribution.

ACKNOWLEDGMENTS

We thank Grzegorz Rajchel-Mieldzioć and Anna Dawid for useful comments on the manuscript.

[1] J. Biamonte, P. Wittek, N. Pancotti, P. Rebentrost, N. Wiebe, and S. Lloyd, Quantum machine learning, *Nature* **549**, 195 (2017).

[2] M. Schuld and F. Petruccione, *Machine Learning with Quantum Computers*, 2nd ed. (Springer, Cham, 2021).

[3] V. Dunjko and P. Wittek, A non-review of quantum machine learning: trends and explorations, *Quantum Views* **4**, 32 (2020).

[4] A. Dawid, J. Arnold, B. Requena, A. Gresch, M. Płodzień, K. Donatella, K. A. Nicoli, P. Stornati, R. Koch, *et al.*, *Machine Learning in Quantum Sciences* (Cambridge University Press, Cambridge, 2024).

[5] C. Conti, *Quantum Machine Learning: Thinking and Exploration in Neural Network Models for Quantum Science and Quantum Computing* (Springer, Cham, 2024).

[6] M. Cerezo, A. Arrasmith, R. Babbush, S. C. Benjamin, S. Endo, K. Fujii, J. R. McClean, K. Mitarai, X. Yuan, L. Cincio, and P. J. Coles, Variational quantum algorithms, *Nature Reviews Physics* **3**, 625 (2021).

[7] Y. Wang and J. Liu, A comprehensive review of quantum machine learning: from NISQ to fault tolerance, *Reports on Progress in Physics* **87**, 116402 (2024).

[8] Y. Guju, A. Matsuo, and R. Raymond, Quantum machine learning on near-term quantum devices: Current state of supervised and unsupervised techniques for real-world applications, *Physical Review Applied* **21**, 067001 (2024).

[9] D. Peral-García, J. Cruz-Benito, and F. J. García-Péñalo, Systematic literature review: Quantum machine learning and its applications, *Computer Science Review* **51**, 100619 (2024).

[10] M. Benedetti, D. García-Pintos, O. Perdomo, V. Leyton-Ortega, Y. Nam, and A. Perdomo-Ortiz, A generative modeling approach for benchmarking and training shallow quantum circuits, *npj Quantum Information* **5**, 45 (2019).

[11] C. Zoufal, *Generative Quantum Machine Learning*, Ph.D. thesis, ETH Zurich (2021), arXiv:2111.12738.

[12] S. Kasture, O. Kyriienko, and V. E. Elfving, Protocols for classically training quantum generative models on probability distributions, *Physical Review A* **108**, 042406 (2023).

[13] A. Delgado and K. E. Hamilton, Quantum generative models, in *Quantum Machine Learning* (IOP Publishing, 2025).

[14] C.-S. Chen, W. A. Hou, H.-W. Hu, and Z.-S. Cai, Quantum generative models for image generation: Insights from MNIST and MedMNIST, arXiv preprint arXiv:2504.00034 (2025).

[15] P.-L. Dallaire-Demers and N. Killoran, Quantum generative adversarial networks, *Physical Review A* **98**, 012324 (2018).

[16] C. Zoufal, A. Lucchi, and S. Woerner, Quantum generative adversarial networks for learning and loading random distributions, *npj Quantum Information* **5**, 103 (2019).

[17] M. Y. Niu, A. Shakeri, A. Lupascu, B. Ghorbani, and J. Zou, Entangling quantum generative adversarial networks, *Physical Review Letters* **128**, 220505 (2022).

[18] X. Gao, E. R. Anschuetz, S.-T. Wang, J. I. Cirac, and M. D. Lukin, Enhancing generative models via quantum correlations, *Physical Review X* **12**, 021037 (2022).

[19] M. Parigi, S. Martina, A. Ferraro, G. García-Pérez, and S. Maniscalco, Quantum diffusion models, arXiv preprint arXiv:2401.06740 (2024).

[20] Y. Li, J. Chen, T. S. Kumavat, and K. Flouris, A purely quantum generative modeling through unitary scrambling and collapse, arXiv preprint arXiv:2506.10571 (2025).

[21] J.-G. Liu and L. Wang, Differentiable learning of quantum circuit Born machines, *Physical Review A* **98**, 062324 (2018).

[22] S. Cheng, J. Chen, and L. Wang, Information perspective to probabilistic modeling: Boltzmann machines versus Born machines, *Entropy* **20**, 583 (2018).

[23] B. Coyle, D. Mills, V. Sherrill, V. Sherrill, V. Sherrill, V. Sherrill, and A. Datta, The Born supremacy: quantum advantage and training of an Ising Born machine, *npj Quantum Information* **6**, 60 (2020).

[24] X. Gao, Z. Zhang, and L. Duan, A quantum machine learning algorithm based on generative models, *Science Advances* **4**, eaat9004 (2018).

[25] M. S. Rudolph, S. Lerch, S. Thanansilp, O. Kiss, O. Ramundo, S. Vallecorsa, and Z. Holmes, Trainability barriers and opportunities in quantum generative modeling, *npj*

Quantum Information **10**, 116 (2024).

[26] K. Gili, M. Hibat-Allah, M. Mauri, C. Ballance, and A. Perdomo-Ortiz, Evaluating generalization in quantum machine learning via leave-one-out cross-validation, Physical Review Research **6**, 013193 (2024).

[27] C. A. Riofrío, O. Mitevski, C. Jones, F. Fuentes, A. Udagawa, and B. Sherbert, A performance characterization of quantum generative models, arXiv preprint arXiv:2301.09363 (2024).

[28] K. Gili, M. Hibat-Allah, M. Mauri, C. Ballance, and A. Perdomo-Ortiz, Do quantum circuit Born machines generalize?, Physical Review A **109**, 012432 (2024).

[29] J. R. McClean, S. Boixo, V. N. Smelyanskiy, R. Babbush, and H. Neven, Barren plateaus in quantum neural network training landscapes, Nature Communications **9**, 4812 (2018).

[30] M. Cerezo, A. Sone, T. Volkoff, L. Cincio, and P. J. Coles, Cost function dependent barren plateaus in shallow parametrized quantum circuits, Nature Communications **12**, 1791 (2021).

[31] Z. Holmes, K. Sharma, M. Cerezo, and P. J. Coles, Connecting ansatz expressibility to gradient magnitudes and barren plateaus, PRX Quantum **3**, 010313 (2022).

[32] S. Sim, P. D. Johnson, and A. Aspuru-Guzik, Expressibility and entangling capability of parameterized quantum circuits for hybrid quantum-classical algorithms, Advanced Quantum Technologies **2**, 1900070 (2019).

[33] Y. Du, Z. Tu, X. Yuan, and D. Tao, Efficient measure for the expressivity of variational quantum algorithms, Physical Review Letters **128**, 080506 (2022).

[34] P. Hayden and J. Preskill, Black holes as mirrors: quantum information in random subsystems, Journal of High Energy Physics **2007**, 120 (2007).

[35] Y. Sekino and L. Susskind, Fast scramblers, Journal of High Energy Physics **2008**, 065 (2008).

[36] B. Swingle, Unscrambling the physics of out-of-time-order correlators, Nature Physics **14**, 988 (2018).

[37] P. Hosur, X.-L. Qi, D. A. Roberts, and B. Yoshida, Chaos in quantum channels, Journal of High Energy Physics **2016**, 4 (2016).

[38] G. Lo Monaco, L. Innocenti, D. Cilluffo, D. A. Chisholm, S. Lorenzo, and G. M. Palma, An operational definition of quantum information scrambling, Quantum Science and Technology **10**, 015039 (2025).

[39] M. Płodzień, Lecture notes on information scrambling, quantum chaos, and haar-random states, arXiv preprint arXiv:2511.14397 (2025).

[40] D. N. Page, Average entropy of a subsystem, Physical Review Letters **71**, 1291 (1993).

[41] H.-Y. Huang, Y. Tong, D. Fang, and Y. Su, Learning many-body Hamiltonians with Heisenberg-limited scaling, Physical Review Letters **130**, 200403 (2023).

[42] W. Yu, J. Sun, Z. Han, and X. Yuan, Robust and efficient Hamiltonian learning, Quantum **7**, 1045 (2023).

[43] A. Dutkiewicz, T. E. O'Brien, and T. Schuster, The advantage of quantum control in many-body Hamiltonian learning, Quantum **8**, 1537 (2024).

[44] A. Gu, L. Cincio, and P. J. Coles, Practical Hamiltonian learning with unitary dynamics and Gibbs states, Nature Communications **15**, 312 (2024).

[45] C. Kokail, B. Sundar, T. V. Zache, A. Elben, B. Vermersch, M. Dalmonte, R. van Bijnen, and P. Zoller, Quantum variational learning of the entanglement Hamiltonian, Physical Review Letters **127**, 170501 (2021).

[46] T. Heightman, E. Jiang, and A. Acín, Solving the quantum many-body Hamiltonian learning problem with neural differential equations, Quantum Science and Technology **10**, 015054 (2025).

[47] T. Olsacher, D. Stilck França, and B. Vermersch, Hamiltonian and Liouvillian learning in weakly-dissipative quantum many-body systems, Quantum Science and Technology **10**, 015062 (2025).

[48] G. Franceschetto, E. Pagliaro, L. Pereira, L. Zambrano, and A. Acín, Hamiltonian learning via quantum Zeno effect (2025), arXiv:2509.15713 [quant-ph].

[49] B. Baran and T. Heightman, Heisenberg-limited quantum Hamiltonian learning via randomly spread product-states (2025), arXiv:2507.21374 [quant-ph].

[50] S.-A. Guo, Y. Wu, J. Ye, L. Zhang, and L.-M. Duan, Hamiltonian learning for 300 trapped ion qubits with long-range couplings, Science Advances **11**, ead4713 (2025).

[51] T. Kraft, M. K. Joshi, W. Lam, T. Olsacher, F. Kranzl, J. Franke, L. K. Joshi, R. Blatt, A. Smerzi, D. Stilck França, B. Vermersch, B. Kraus, C. F. Roos, and P. Zoller, Bounded-error quantum simulation via Hamiltonian and Lindbladian learning (2025), arXiv:2511.23392 [quant-ph].

[52] A. A. Mele, Introduction to haar measure tools in quantum information: A beginner's tutorial, Quantum **8**, 1340 (2024).

[53] I. Bengtsson and K. Życzkowski, *Geometry of Quantum States: An Introduction to Quantum Entanglement*, 2nd ed. (Cambridge University Press, Cambridge, 2017).

[54] P. Hayden, D. W. Leung, and A. Winter, Aspects of generic entanglement, Communications in Mathematical Physics **265**, 95 (2006).

[55] K. Życzkowski and H.-J. Sommers, Induced measures in the space of mixed quantum states, J. Phys. A: Math. Gen. **34**, 7111 (2001).

[56] F. Mezzadri, How to generate random matrices from the classical compact groups, Notices of the American Mathematical Society **54**, 592 (2007).

[57] A. W. Harrow and R. A. Low, Random quantum circuits are approximate 2-designs, Communications in Mathematical Physics **291**, 257 (2009).

[58] F. G. S. L. Brandão, A. W. Harrow, and M. Horodecki, Local random quantum circuits are approximate polynomial-designs, Communications in Mathematical Physics **346**, 397 (2016).

[59] J. Haah, Y.-A. Liu, and X. Tan, Efficient approximate unitary designs from random pauli rotations, in *2024 IEEE 65th Annual Symposium on Foundations of Computer Science (FOCS)* (IEEE, 2024) pp. 568–581.

[60] A. W. Harrow and S. Mehraban, Approximate unitary t -designs by short random quantum circuits using nearest-neighbor and long-range gates, Communications in Mathematical Physics **401**, 1531 (2023).

[61] B. Fefferman, S. Ghosh, and W. Zhan, Anti-concentration for the unitary haar measure and applications to random quantum circuits, arXiv preprint arXiv:2407.19561 (2024).

[62] B. Foxman, N. Parham, F. Vasconcelos, and H. Yuen, Random unitaries in constant (quantum) time, arXiv preprint arXiv:2508.11487 (2025), analyzes $\Theta(\log \log n)$ and constant-depth designs using nonlocal gates like Fanout or Toffoli.

- [63] J. Emerson, Y. S. Weinstein, M. Saraceno, S. Lloyd, and D. G. Cory, Pseudo-random unitary operators for quantum information processing, *Science* **302**, 2098 (2003).
- [64] J. Maldacena, S. H. Shenker, and D. Stanford, A bound on chaos, *Journal of High Energy Physics* **2016**, 106 (2016).
- [65] T. M. Cover and J. A. Thomas, *Elements of Information Theory*, 2nd ed. (Wiley-Interscience, 2006).
- [66] D. P. Kingma and J. Ba, Adam: A method for stochastic optimization, *Proceedings of the 3rd International Conference on Learning Representations (ICLR)* (2015).
- [67] T. Giamarchi, *Quantum Physics in One Dimension* (Oxford University Press, 2003).
- [68] S. J. Prince, *Understanding Deep Learning* (MIT Press, 2023).
- [69] I. Goodfellow, J. Pouget-Abadie, M. Mirza, B. Xu, D. Warde-Farley, S. Ozair, A. Courville, and Y. Bengio, Generative adversarial nets, in *Advances in Neural Information Processing Systems*, Vol. 27 (2014).
- [70] D. P. Kingma and M. Welling, Auto-encoding variational Bayes, arXiv preprint arXiv:1312.6114 (2014).
- [71] G. E. Hinton, A practical guide to training restricted Boltzmann machines, *Neural Networks: Tricks of the Trade*, 599 (2012).
- [72] GAN: Adam, lr = 2×10^{-4} , $\beta_1 = 0.5$, MLP with $H = 13$ (302 params) [69]; VAE: Adam, lr = 10^{-3} , $\beta = 0.1$, $H = 25$ (306 params) [70]; RBM: SGD, lr = 10^{-2} , CD-1, $H = 102$ (308 params) [71].
- [73] A. Sannia, R. Martínez-Peña, M. C. Soriano, G. L. Giorgi, and R. Zambrini, Dissipation as a resource for quantum reservoir computing, *Quantum* **8**, 1291 (2024).